https://doi.org/10.5194/egusphere-2026-5836
Preprint. Discussion started: 3 November 2026
© Author(s) 2026. CC BY 4.0 License.

Development of a lightweight broadband cavity-enhanced spectrometer system for simultaneous monitoring of HONO and NO_2

Yilan Li[1], Caroline C. Womack[2], Nell B. Schafer[2, 3, 4], Jiajue Chai[1]

[1]Department of Chemistry, State University of New York, College of Environmental Science and Forestry, Syracuse, NY
[2]Chemical Sciences Laboratory, National Oceanic and Atmospheric Administration, Boulder, CO 80305, USA
[3]Cooperative Institute for Research in Environmental Sciences, University of Colorado, Boulder, CO 80309, USA
[4]Department of Chemistry, University of Colorado, Boulder, CO 80309, USA

Correspondence to: Jiajue Chai (jichai@esf.edu)

Abstract. Nitrous acid (HONO) is an important source of hydroxyl radicals in the troposphere, but its measurement remains challenging because of its low atmospheric abundance and rapid temporal variability. In this work, we developed a compact broadband cavity-enhanced absorption spectrometer (BBCEAS) for simultaneous measurements of HONO and NO_2 in the near-UV spectral region. The instrument uses a high-reflectivity optical cavity, with a measured mirror reflectivity of 0.99986 at 368 nm, and a spectral acquisition time of 0.15 s. Laboratory characterization demonstrated stable and sensitive measurements of both species. The instrument achieved 1σ precisions of 193 pptv for HONO and 584 pptv for NO_2 at 1 s time resolution, improving to 30 pptv and 76 pptv, respectively, at a 60 s averaging time. Intercomparison measurements showed excellent agreement with reference analyzers, with nearly unit regression slopes for both HONO and NO_2. Controlled humidity experiments showed no systematic dependence of the retrieved concentrations on water vapour over the investigated range, indicating robust performance under varying humidity conditions. In addition, a 24 h ambient deployment in Syracuse, New York, USA, demonstrated the practical applicability of the instrument for continuous measurements of atmospheric HONO and NO_2. The instrument provided high-temporal-resolution measurements of HONO and NO_2 and enabled continuous measurements of HONO at 10s of pptv levels. The combination of high sensitivity, rapid acquisition, compact design, and stable performance provides potential for continuous monitoring across diverse environments and for integration with mobile and airborne platforms.

1 Introduction

Nitrous acid (HONO) is an important component of tropospheric chemistry because its photolysis produces hydroxyl radicals (OH), a primary atmospheric oxidant that initiates the oxidation of volatile organic compounds (VOCs), carbon monoxide (CO), and numerous trace gases (Alicke et al., 2003; Kleffmann, 2007). Consequently, HONO can substantially influence atmospheric oxidative capacity and the formation of secondary pollutants, including ozone (O_3) and secondary aerosols (Kleffmann, 2007; Wang et al., 2025a). Field observations and modeling studies have demonstrated that HONO photolysis can contribute substantial daytime OH production, particularly during the early morning when other

https://doi.org/10.5194/egusphere-2026-5836
Preprint. Discussion started: 3 November 2026
© Author(s) 2026. CC BY 4.0 License.

photochemical radical sources remain weak (Alicke et al., 2003; Andersen et al., 2023; Kleffmann, 2007). Currently, substantial uncertainties remain in the atmospheric HONO budget, and observed HONO concentrations frequently exceed model predictions, suggesting that important HONO sources and chemical processes remain insufficiently represented, particularly those involving heterogeneous reactions, surface photochemistry, and multiphase NO_x conversion (Kim et al., 2024; Kleffmann, 2007; Wang et al., 2025a; Zhang et al., 2023). Given its central role in atmospheric oxidation chemistry, accurate, precise, and fast-response HONO measurement with field portability is essential for understanding photochemical processes and improving air quality model predictions.

Nitrogen dioxide (NO_2) is a major precursor to HONO. Heterogeneous conversion of NO_2 on the ground surfaces, aerosols, and other environmental interfaces in the absence and presence of sunlight has long been recognized as an important source of atmospheric HONO (Aubin and Abbatt, 2007; Bao et al., 2022; Finlayson-Pitts et al., 2003; Kleffmann, 2007; Stemmler et al., 2006; Wang et al., 2025a). Simultaneous measurements of HONO and NO_2 can therefore provide constraints on HONO formation mechanisms and reactive nitrogen cycling. Owing to the strong chemical coupling between these species, the HONO/NO_2 ratio has been widely used as a diagnostic metric for evaluating HONO formation and atmospheric processing. Variations in this ratio can help distinguish direct emissions from secondary HONO formation and provide useful constraints for evaluating chemical transport models and HONO parameterizations (Kim et al., 2024; Kleffmann, 2007; Wang et al., 2025a).

Atmospheric HONO measurements remain challenging because ambient concentrations typically range from several tens of pptv to a few ppbv and exhibit pronounced temporal and spatial variability. In addition, HONO is highly reactive and susceptible to wall losses and secondary formation during sampling, making accurate quantification difficult under field conditions (Kleffmann, 2007; Pinto et al., 2014; Wang et al., 2025a).

To address these challenges, a variety of techniques have been developed for HONO observations, including long-path absorption photometry (LOPAP), denuder-based methods, chemical ionization mass spectrometry (CIMS), differential optical absorption spectroscopy (DOAS), cavity ring-down spectroscopy (CRDS), and cavity-enhanced absorption spectroscopy (CEAS) (Crilley et al., 2019; Pinto et al., 2014; Wang et al., 2025b). Among these approaches, LOPAP is widely used as a sensitive and selective technique for atmospheric HONO measurements and has been extensively applied in atmospheric field measurements (Crilley et al., 2019; Heland et al., 2001). However, wet-chemical methods generally require consumable reagents, regular maintenance, and relatively complex sampling systems. Furthermore, inlet interactions and heterogeneous chemical conversion may introduce measurement artifacts, particularly during long-term unattended operation and mobile deployments (Crilley et al., 2019; Wang et al., 2025b). CIMS provides high sensitivity and rapid time response, making it well suited for investigating fast atmospheric processes (Roberts et al., 2010; Veres et al., 2008). However, its operation relies on reagent ions and relatively complex instrumentation, which may increase operational complexity and susceptibility to chemical interferences (Pinto et al., 2014; Wang et al., 2025b). Optical absorption techniques provide a reagent-free alternative with minimal sample handling, thereby avoiding several artifacts associated with wet-chemical sampling. Among these methods, broadband cavity-enhanced absorption spectroscopy (BBCEAS) is well

https://doi.org/10.5194/egusphere-2026-5836
Preprint. Discussion started: 3 November 2026
© Author(s) 2026. CC BY 4.0 License.

suited to atmospheric trace-gas measurements because it combines high sensitivity, broad spectral coverage, and continuous operation capability. In the near-ultraviolet spectral region, HONO and NO_2 can be simultaneously retrieved from a single broadband absorption spectrum, allowing simultaneous measurements of two chemically coupled species with the same optical path and sampling system. Previous studies have successfully applied BBCEAS techniques to HONO and NO_2 measurements under both laboratory and field conditions (Duan et al., 2018; Tang et al., 2020; Wu et al., 2012). More recent developments have extended cavity-enhanced measurements to mobile platforms and emission characterization studies while further improving HONO quantification capabilities (Harper et al., 2025; Wang et al., 2025b).

Despite these advances, the size, weight, and power requirements of BBCEAS instruments remain important considerations for many field applications. Recent advances in compact UV LEDs, miniaturized spectrometers, lightweight optical components, and low-power electronics have enabled increasingly portable designs and expanded the use of BBCEAS for field and mobile measurements (Duan et al., 2018; Harper et al., 2025; Wang et al., 2025b). Nevertheless, relatively few studies have specifically focused on developing lightweight, low-power, and highly portable BBCEAS instruments capable of sensitive, simultaneous measurements of HONO and NO_2.

Motivated by these needs, we developed a lightweight and portable BBCEAS instrument for simultaneous measurements of HONO and NO_2. The instrument builds upon the compact cavity-enhanced spectrometer concept demonstrated by Womack et al. (2022) for NO_2 measurements on uncrewed aerial systems and extends the platform to simultaneous HONO and NO_2 measurements. The instrument combines high sensitivity and fast response with low power consumption and compact dimensions while maintaining continuous measurement capability. We evaluated the performance of our BBCEAS using a laboratory-generated HONO source and standard NO_2 gas addition to characterize its precision, stability, humidity dependence, and measurement accuracy. We also performed continuous ambient measurements to assess its capability for field deployment and performance.

2 Instrument design

Broadband cavity-enhanced absorption spectroscopy (BBCEAS) is a highly sensitive optical absorption technique that has been widely employed for in situ measurements of trace gases and aerosol extinction in the ultraviolet and visible spectral regions (Fiedler et al., 2003; Langridge, 2008; Washenfelder et al., 2008). A BBCEAS instrument typically combines a broadband light source with a high-reflectivity optical cavity, providing effective path lengths of several kilometers and enabling simultaneous retrieval of multiple light-absorbing atmospheric species through spectral fitting. Previous studies have demonstrated the successful application of BBCEAS systems in ground-based, mobile, and airborne measurements of reactive nitrogen species, particularly NO_2 and HONO, with high sensitivity and temporal resolution (Duan et al., 2018; Gherman et al., 2008; Kennedy et al., 2011; Min et al., 2016; Wu et al., 2012). Building upon these advances, this work develops a miniaturized BBCEAS instrument capable of simultaneous HONO and NO_2 measurements. The system was specifically designed to provide a lightweight and compact solution for high-precision atmospheric observations in space-

https://doi.org/10.5194/egusphere-2026-5836
Preprint. Discussion started: 3 November 2026
© Author(s) 2026. CC BY 4.0 License.

and payload-constrained environments. Briefly, the BBCEAS developed in this study consists of the optical system, flow system, electrical system, data acquisition system, and mechanical system, each of which is described in detail in the following sections.

2.1 Optical system

The optical system of the BBCEAS instrument, illustrated by the blue dashed box in Figure 1(a), primarily comprises a light-emitting diode (LED) source, an off-axis parabolic mirror, a high-finesse optical cavity equipped with two high-reflectivity dielectric mirrors, a convex collection lens, a bandpass filter, an optical fiber, and a miniature grating spectrometer. The light source is a violet LED (LST1-01G01-UV01-00, New Energy) with a central wavelength of 365 nm. The LED is a chip-on-board (COB) module from the SST-10 series, mounted on a starboard substrate. Under typical operating conditions, the LED exhibits an optical output power of 875 mW at a drive current of 500 mA and a temperature of 25 °C. The forward voltage is approximately 3.6 V, and the emission is characterized by a viewing angle of 130°. To minimize spectral drift and intensity fluctuations during field operation, the LED is temperature stabilized at 22.50 ± 0.05 °C using a thermoelectric cooler (TEC; CP60233, CUI Devices, Tualatin, OR, USA). The emitted radiation is collected and collimated by an off-axis parabolic mirror (50328AL, Newport Corp., Irvine, CA, USA) with a diameter of 1.50 inches and an effective focal length of 0.80 inches. The collimated beam is subsequently coupled into a high-reflectivity optical cavity formed by two dielectric mirrors (FiveNines Optics, Boulder, CO, USA) with a diameter of 2.5 cm and a radius of curvature of 0.5 m. The cavity mirrors exhibit a measured reflectivity of 0.99986 at 368 nm, corresponding to an effective absorption path length of approximately 1.6 km and enabling sensitive detection of HONO and NO_2. Light transmitted through the cavity is filtered using a 370/36 nm Bright Line® single-band bandpass filter to suppress stray light and unwanted spectral contributions outside the target wavelength region. The filtered light is subsequently focused by a convex lens with a focal length of 50 mm into a 1 m-long circular optical fiber (600 μm core diameter; Ocean Insight Inc., Dunedin, FL, USA), which guides the transmitted radiation to the detection system. Spectral measurements are performed using a compact grating spectrometer (QE Pro; Ocean Insight Inc., Dunedin, FL, USA) equipped with a 200 μm-wide entrance slit and configured with a holographic grating (1800 lines mm-1) optimized for near-UV measurements. The spectrometer is based on a thermoelectrically cooled, back-thinned CCD detector (Hamamatsu S7031 series) with a typical pixel array of 1044 × 64 elements, providing high quantum efficiency and low-noise performance. According to the factory wavelength calibration, the spectrometer covers the spectral range from approximately 309 to 424 nm, encompassing the absorption features of both HONO and NO_2 used in this study. The spectral resolution is approximately 0.9-1.3 nm with the 200 μm entrance slit. Each spectrum is acquired with an integration time of 0.15 s, which provides sufficient detector signal while avoiding saturation under typical operating conditions. Additional features of the spectrometer include onboard spectral buffering (up to ~15,000 spectra), a signal-to-noise ratio on the order of 1000:1 (single scan), and integration times ranging from milliseconds to minutes, enabling flexible operation under varying light levels. Although the QE Pro provides lower spectral resolution than larger laboratory-grade spectrometers, its compact dimensions (182 × 110 × 47 mm), low weight (approximately 1.15 kg), thermoelectrically cooled detector, and rapid spectral

https://doi.org/10.5194/egusphere-2026-5836
Preprint. Discussion started: 3 November 2026
© Author(s) 2026. CC BY 4.0 License.

acquisition capability (0.15 s per spectrum) make it well suited for mobile applications requiring high-temporal-resolution measurements under rapidly changing atmospheric conditions.

To ensure stable optical alignment under stationary, mobile, and airborne operating conditions, the cavity mirrors and optical components were mounted within a rigid mechanical framework designed to minimize vibration-induced displacement. Initial optical alignment was performed using a low-power visible alignment laser, followed by fine adjustment of the cavity mirrors to maximize cavity throughput and spectral signal intensity. The compact optical architecture, together with the lightweight spectrometer and low-power electronics, enables high-sensitivity measurements in a compact and lightweight package suitable for routine field deployment.

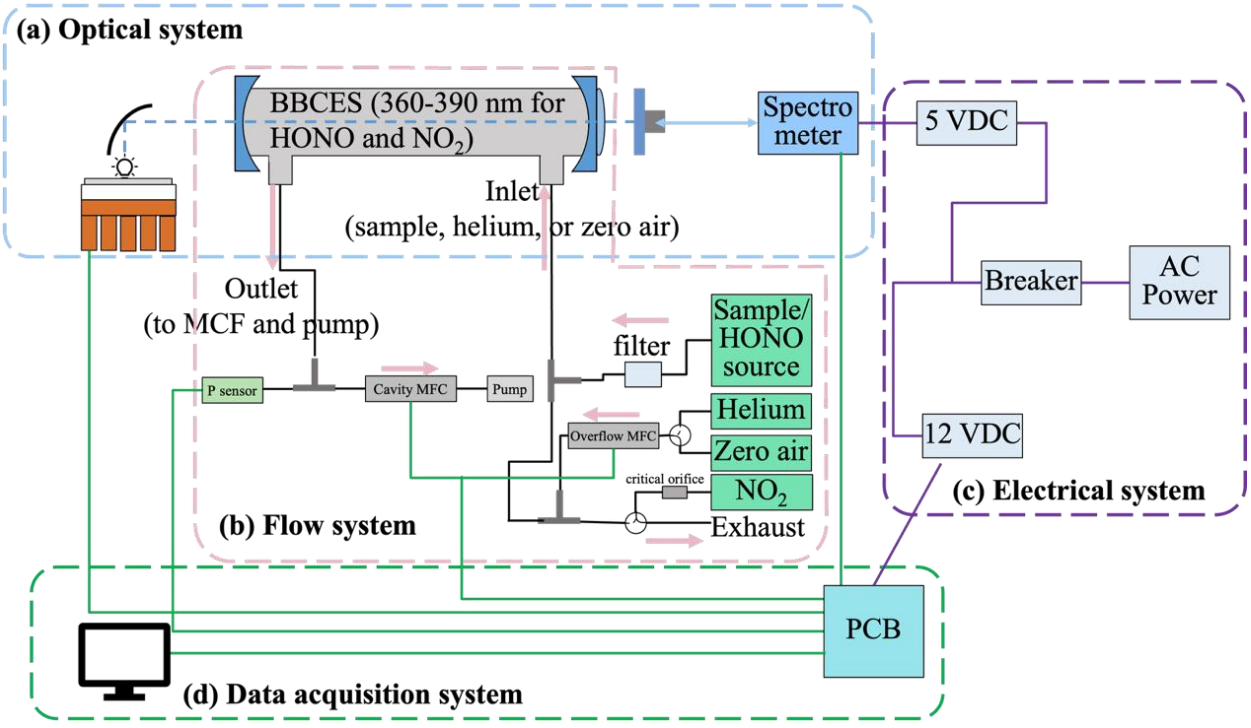


Figure 1: Schematic of the instrument, showing the optical (a), flow (b), electrical (c), and data acquisition (d) systems.

2.2 Flow system

The flow system of our miniature BBCEAS, highlighted by the pink dashed region in Figure 1(b), consists of a particulate filter, an optical cavity, pressure and flow sensors, and a diaphragm pump. Sample air first passes through a filter pack (Savillex, Eden Prairie, MN, USA) equipped with a replaceable 0.45 µm-pore polytetrafluoroethylene (PTFE) filter (Savillex, Eden Prairie, MN, USA) to minimize particulate contamination of the optical cavity and mirror surfaces. The optical cavity is fabricated from PTFE tubing with an inner diameter of 1/2″. Sample air enters and exits the cavity through PTFE fittings and is transported to the instrument through 1/4″ OD PTFE tubing. Previous studies have shown that losses of HONO and NO_2 on fluoropolymer surfaces are generally low under typical atmospheric sampling conditions (Min et al., 2016;

https://doi.org/10.5194/egusphere-2026-5836
Preprint. Discussion started: 3 November 2026
© Author(s) 2026. CC BY 4.0 License.

Gingerysty and Osthoff, 2020). To minimize potential sampling artifacts, all wetted surfaces in the sampling line were constructed from PTFE materials. High-reflectivity cavity mirrors are mounted on aluminum plates and sealed with O-rings to ensure leak-tight operation. Following the design adopted by Womack et al. (2022), no mirror-purge flow is employed. Although mirror purging can reduce contamination of optical surfaces, it requires a continuous supply of particle-free zero air, increasing the size, weight, and power requirements of the instrument. In the absence of mirror purging, mirror cleanliness is maintained through periodic inspection of the cavity reflectivity (Sect. 3.2). Mirrors are removed and cleaned when a significant decrease in reflectivity (below 0.9998) is observed, typically at intervals of approximately one month during routine laboratory operation, although more frequent maintenance may be necessary in heavily polluted environments. The cavity pressure is monitored using a miniature pressure sensor (24PCCFA6A, Honeywell, Golden Valley, MN, USA). Sample flow is regulated by a mass flow controller (Basis 2.0 MEMS, Alicat Scientific, Tucson, AZ, USA), with a flow range of 0-5 standard liters per minute (SLPM), RS-485 communication (Alicat ASCII/Modbus RTU), and 0-5 V analog input/output under standard conditions (25 °C, 1 atm). At the nominal sample flow rate of 1 L min-1, the 28.5 cm^3 PTFE cavity provides a gas residence time of approximately 1.7 s. The tubing between the filter pack and the cavity is approximately 30 cm long, corresponding to an internal volume of approximately 2.4 cm^3 and a residence time of approximately 0.15 s. Therefore, the inlet residence time contributes only a minor fraction of the overall sampling response time. Gas number density in the cavity is calculated from the measured pressure and temperature using the ideal gas law. Sample temperature is approximated by the ambient temperature and monitored continuously using a thermistor mounted on the external cavity wall.

2.3 Electrical system

The electrical subsystem (Figure 1(c)) supplies power to the LED, TEC, cooling fan, and spectrometer. A power management module distributes the required operating voltages to the individual components. For laboratory, mobile laboratory, and ground-based field deployments, the instrument is powered directly from an external alternating current AC source. The instrument can alternatively be powered by a rechargeable 14.8 V lithium-ion battery pack (32.56 Wh, 4 A Rate; 31021, Tenergy Corp., Fremont, CA, USA). Regardless of the power source, the internal power management circuitry regulates and distributes the required operating voltages (12 and 5 V) to the instrument subsystems. To ensure operational safety, the AC input is protected by a circuit breaker, and the instrument enclosure is electrically grounded. Power consumption varies with ambient temperature and operating conditions due to the active temperature control of both the LED and detector. For deployments where AC power is unavailable, the instrument can also be operated using an external battery pack.

2.4 Data acquisition system

The data acquisition and control system (Figure 1(d)) is centered on a custom printed circuit board (PCB), which serves as the primary interface for power distribution, signal acquisition, and subsystem integration. The PCB distributes regulated

https://doi.org/10.5194/egusphere-2026-5836
Preprint. Discussion started: 3 November 2026
© Author(s) 2026. CC BY 4.0 License.

supply voltages to key components, including the LED, TEC, cooling fan, and auxiliary electronics. In parallel, it acquires analog and digital signals from temperature sensors (cavity and box), as well as from the pressure sensor, while digital interfaces enable real-time communication with external devices. The PCB provides RS-485 communication for peripheral subsystems such as mass flow controllers (MFCs), allowing coordinated operation of the gas-handling system. It also routes control signals to actuation elements (e.g., valves or solid-state relays), enabling synchronized regulation of gas flows and operating states. A secondary interface board mounted on the main PCB expands communication channels and facilitates signal routing between internal components and external hardware. The TEC is controlled by a Peltier controller module (TEC-1092; Meerstetter Engineering GmbH, Switzerland) integrated with the PCB. This controller communicates with the control computer via a serial interface, enabling continuous monitoring of LED temperature and TEC operating current. A compact single-board computer running Linux (BeagleBone Black Rev C; BeagleBoard.org, USA) performs high-level instrument control, data logging, and system coordination. Data acquisition is implemented with custom-built Python software, with spectrometer operation controlled via the Ocean Insight SeaBreeze API (v3.0.11). The system acquires measurements of LED temperature, ambient temperature, sample pressure, sample flow, and optical spectra with an integration time of 0.15 s and averages them to a temporal resolution of 1 s. The effective time response is primarily limited by the gas residence time in the optical cavity (~1.2 s). During ground-based operation, the instrument is monitored using a custom-built LabVIEW user interface operated on a separate laptop, enabling real-time monitoring and control.

2.5 Mechanical system

The optical and flow components of the instrument are mounted on a frame constructed from hollow carbon fiber rods (1.27 cm diameter; GR-CFR-TUBE-0.500OD, GraphiteStore, USA). Optical elements are fixed to custom-machined aluminum plates (0.76 cm thickness), which are rigidly attached to the carbon fiber framework to ensure mechanical stability. Instrument performance is sensitive to optical alignment; therefore, all adjustable components are locked in place after alignment using screws or other mechanical fasteners to minimize drift during operation. The optical assembly, PCB, spectrometer, and power conversion modules are housed within a standard 19″ rack box (20″ depth, ~5.2″ height) and mounted on aluminum rails. This configuration provides mechanical support while facilitating modular integration and maintenance. The complete BBCEAS instrument weighs approximately 19 lb (9 kg), making it suitable for portable field deployment.

2.6 Laboratory HONO generation system

A laboratory HONO source was used for instrument characterization and performance evaluation. HONO was generated through proton-transfer acid displacement using hydrochloric acid (HCl) and sodium nitrite ($NaNO_2$), following the approach described by Lao et al. (2020). A controlled HCl flow was introduced into a nitrite-containing reactor, producing gas-phase HONO that was subsequently diluted with particle-free air to the desired concentration. The source provided

https://doi.org/10.5194/egusphere-2026-5836
Preprint. Discussion started: 3 November 2026
© Author(s) 2026. CC BY 4.0 License.

stable and reproducible HONO mixing ratios over a range relevant to atmospheric measurements and was used for reflectivity calibration, sensitivity assessment, and instrument validation experiments.

2.7 Field deployment

Field measurements were conducted on the rooftop of Baker Laboratory at the SUNY College of Environmental Science and Forestry (SUNY ESF) main campus in Syracuse, New York, USA (43.03° N, 76.14° W). The sampling inlet was installed approximately 20 m above ground level. The site is located on the southeastern side of downtown Syracuse and approximately 400 m east (upwind) of Interstate 81 (I-81), a major north-south transportation corridor. The measurement location is representative of a mid-sized urban environment influenced primarily by urban background air from the Syracuse metropolitan area. The location of the sampling site is shown in Figure 2.



Figure 2: Location of the rooftop ambient sampling site at Baker Laboratory on the SUNY College of Environmental Science and Forestry (SUNY ESF) campus in Syracuse, New York, USA. The sampling location is indicated by the red point. Interstate 81 (I-81) is shown for reference (Base map: Esri and its data providers | Powered by Esri).

https://doi.org/10.5194/egusphere-2026-5836
Preprint. Discussion started: 3 November 2026
© Author(s) 2026. CC BY 4.0 License.

3 Data analysis

3.1 Wavelength calibration

Accurate wavelength assignment is critical for BBCEAS because measured transmission spectra must be aligned with the reference absorption cross sections used for spectral retrieval. Wavelengths were assigned to detector pixels using the factory calibration coefficients provided by Ocean Insight (Eq. (1)):

$$\lambda(x)=309.725+0.12181x-(9.37944\times10^{-6})x, \quad (1)$$

where λ(x) is the wavelength (nm), x is the detector pixel number. This calibration function describes the wavelength dispersion of the spectrometer and assigns a wavelength coordinate to each detector pixel across the recorded spectral range. Before spectral fitting, the wavelength-calibrated spectra are corrected for detector dark current by subtracting dark spectra acquired with the same integration time and detector settings while the LED light source is switched off. The processed spectra are subsequently used for BBCEAS spectral retrieval.

3.2 Mirror reflectivity

The wavelength-dependent mirror reflectivity, R(λ), is a key parameter for determining the effective optical path length of the BBCEAS cavity and, consequently, the quantitative retrieval of trace-gas concentrations. In this study, R(λ) is determined using the Rayleigh scattering method, which exploits the difference in Rayleigh extinction between two gases with well-characterized scattering cross sections of significantly differing magnitudes (Fiedler et al., 2003; Min et al., 2016; Washenfelder et al., 2008).

High-purity helium (He, 99.999 %) and zero air (ZA) are sequentially introduced into the cavity under identical pressure and flow conditions. Assuming negligible absorption by either gas over the fitting wavelength range, the mirror reflectivity was calculated following Washenfelder et al. (2008):

$$R(\lambda)=1-d\frac{\left[\frac{I_{ZA}(\lambda)}{I_{He}(\lambda)}\alpha_{Ray,ZA}(\lambda)-\alpha_{Ray,He}(\lambda)\right]}{1-\frac{I_{ZA}(\lambda)}{I_{He}(\lambda)}}, \quad (2)$$

In Eq. (2), d is the cavity length, $I_{ZA}(\lambda)$ and $I_{He}(\lambda)$ are the measured intensity spectra obtained with zero air and helium, respectively, and $\alpha_{Ray,ZA}(\lambda)$ and $\alpha_{Ray,He}(\lambda)$ are the corresponding Rayleigh extinction coefficients. Because helium has a Rayleigh scattering cross section that is approximately one order of magnitude lower than that of air in the near-ultraviolet spectral region, the difference in cavity transmission between the two gases provides a direct measure of the mirror reflectivity. The Rayleigh scattering cross sections are calculated following Thalman et al. (2014), which accounts for the wavelength dependence of the refractive index and King correction factor for each gas. The resulting wavelength-dependent mirror reflectivity is subsequently used to calculate the effective optical path length and retrieve trace-gas concentrations from the measured absorption spectra.

https://doi.org/10.5194/egusphere-2026-5836
Preprint. Discussion started: 3 November 2026
© Author(s) 2026. CC BY 4.0 License.

3.3 Total extinction and spectral fitting

The wavelength-dependent extinction coefficient, $\alpha_{ext}(\lambda)$, is calculated from the measured cavity transmission using the wavelength-dependent mirror reflectivity determined in Eq. (2). Following the BBCEAS formalism (Fiedler et al., 2003; Min et al., 2016; Washenfelder et al., 2008), the total extinction coefficient is given by:

$$\alpha_{ext}(\lambda)=\left(\frac{1-R(\lambda)}{d}+\alpha_{Ray,ZA}(\lambda)\right)\left(\frac{I_{ZA}(\lambda)-I_{sample}(\lambda)}{I_{sample}(\lambda)}\right)+\Delta\alpha_{Ray}(\lambda), \quad (3)$$

where $I_{ZA}(\lambda)$ and $I_{sample}(\lambda)$ are the transmitted intensities measured for the reference gas (zero air) and sample spectra, respectively. The term $\Delta\alpha_{Ray}(\lambda)$ accounts for the difference in Rayleigh extinction between the reference and sample conditions arising from variations in gas composition or pressure (Duan et al., 2018).

The measured extinction spectrum is fitted as the sum of the absorption by individual trace gases and a slowly varying broadband background,

$$\alpha_{ext}(\lambda) = \sum_i^n \sigma_i(\lambda) N_i + p(\lambda), \quad (4)$$

where $\sigma_i(\lambda)$ is the absorption cross section, N_i is the corresponding number density of the *i*-th absorber, and $p(\lambda)$ is a fourth-order polynomial accounting for broadband extinction caused by aerosol scattering, LED intensity fluctuations, and residual baseline variations.

HONO and NO_2 are retrieved simultaneously using literature absorption cross sections from Stutz et al. (2000) and Vandaele et al. (1998), respectively. All reference spectra are convolved with the experimentally determined instrument line shape (ILS) and interpolated onto the calibrated wavelength grid before fitting. Spectral fitting is performed over 360-390 nm, which covers the characteristic absorption features of both HONO and NO_2 while providing high signal-to-noise ratios for spectral retrieval (Duan et al., 2018; Tang et al., 2020). The measured extinction spectra are fitted using a nonlinear Levenberg-Marquardt least-squares routine implemented in Igor Pro (WaveMetrics, Lake Oswego, OR, USA), from which HONO and NO_2 concentrations and the polynomial baseline coefficients are obtained simultaneously (Levenberg, 1944; Marquardt, 1963).

3.4 System performance and uncertainty analysis

System precision and optimum averaging time are evaluated using Allan deviation, $\sigma_A(\tau)$, which is widely used to characterize instrument noise and temporal stability in optical trace-gas measurements (Werle et al., 1993; Werle, 2011). Zero air measurements are used to generate continuous time series of retrieved mixing ratios. The Allan deviation is defined as:

$$\sigma_A^2(\tau)=\frac{1}{2(m-1)}\sum_{j=1}^{m-1}(y_{j+1}-y_j)^2, \quad (5)$$

where τ is the averaging time (s), m is the number of consecutive intervals, and y_j denotes the mean concentration in the *j*-th interval.

https://doi.org/10.5194/egusphere-2026-5836
Preprint. Discussion started: 3 November 2026
© Author(s) 2026. CC BY 4.0 License.

For a system dominated by uncorrelated random noise (white noise), the Allan deviation decreases with averaging time according to a $\tau^{-1/2}$ dependence, indicating that measurement precision improves through signal averaging. At longer averaging times, instrumental drift arising from temperature fluctuations, LED intensity variations, and baseline instability becomes increasingly important, causing deviations from this relationship (Werle et al., 1993; Werle, 2011).

The Allan deviation curve can be used to identify an optimal averaging time (τ_{opt}) for a specific application by balancing improvements in measurement precision against the loss of temporal resolution. The corresponding Allan deviation provides an estimate of the achievable instrumental precision under zero air conditions.

Total measurement uncertainty is estimated by considering both systematic and random contributions. Systematic uncertainties arise from mirror reflectivity calibration, absorption cross-section uncertainties, and pressure and temperature measurements. Random uncertainty is estimated from the Allan deviation at the selected averaging time.

4 Results and discussion

4.1 Instrument precision and stability

The precision and short-term stability of the BBCEAS instrument were assessed using an approximately 3 h zero air (ZA) measurement. Figures 3a and 3b show the concentration distributions, while Figures 3c and 3d present the corresponding Allan deviation results, all derived from the same dataset.

The concentration distributions obtained under laboratory ZA conditions were approximately Gaussian for both HONO and NO_2, consistent with measurement variability dominated by random instrumental noise. Gaussian fits gave standard deviations of 198 ppt for HONO and 582 ppt for NO_2 (Figs. 3a and 3b), corresponding to the 1σ measurement precision at 1 s. The fitted mean concentrations were -38 ppt for HONO and -242 ppt for NO_2, indicating small systematic offsets in the retrieved concentrations. These offsets likely reflect residual systematic errors in the spectral retrieval, such as baseline or reference-spectrum uncertainties. Because the offsets primarily affect the mean rather than the width of the concentration distribution, their influence on the precision estimates is negligible. Correction of these offsets is nevertheless important for accurate ambient measurements.

The larger standard deviation for NO_2 indicates lower retrieval precision than for HONO under the same operating conditions. This difference may reflect differences in absorption strength and spectral retrieval sensitivity between the two species. Similar differences in HONO and NO_2 precision have been reported for other BBCEAS instruments (Duan et al., 2018; Tang et al., 2020).

Allan deviation analysis was used to characterize the dependence of measurement precision on averaging time, τ (Figs. 3c and 3d). For both species, the Allan deviation decreased approximately as $\tau^{-1/2}$ from 1 to at least 300 s, consistent with white-noise-dominated measurement variability over this interval (Langridge et al., 2008; Werle et al., 1993). The 1σ Allan deviations for HONO were 193, 39, and 11 ppt at averaging times of 1, 30, and 300 s, respectively, compared with 584, 114, and 35 ppt for NO_2. The Allan deviation followed the expected $\tau^{-1/2}$ dependence throughout this interval, and no minimum

https://doi.org/10.5194/egusphere-2026-5836
Preprint. Discussion started: 3 November 2026
© Author(s) 2026. CC BY 4.0 License.

was observed up to 300 s, suggesting that instrumental drift did not become important on this timescale. Although precision continued to improve with increasing averaging time, longer averaging reduces temporal resolution and may obscure short-term atmospheric variability. An averaging time of 60 s was therefore selected for subsequent measurements as a practical compromise between precision and temporal resolution. Based on the observed $\tau^{-1/2}$ dependence, the corresponding 1σ precisions are estimated to be approximately 30 ppt for HONO and 76 ppt for NO_2.

At 60 s averaging, the corresponding 2σ detection limits are approximately 60 ppt for HONO and 152 ppt for NO_2. Ambient HONO concentrations in urban and suburban environments typically range from several hundred ppt to a few ppb, although lower concentrations may occur in remote regions (Kleffmann et al., 2005; Kleffmann and Wiesen, 2008). These sensitivities are therefore sufficient for most urban and suburban HONO observations and are comparable to those reported for other BBCEAS instruments (Table 1). Duan et al. (2018) reported 2σ precisions of approximately 180 ppt for HONO and 340 ppt for NO_2 at 30 s, whereas Tang et al. (2020) reported Allan-deviation-derived 2σ detection limits of 80 pptv for HONO and 140 pptv for NO_2 at a 60 s integration time. Although BBCEAS instruments operating at longer visible wavelengths can achieve improved NO_2 precision (e.g., Womack et al., 2022, Table 1), the current spectral region enables simultaneous retrieval of both HONO and NO_2. The present instrument therefore provides sensitive measurements of both species within a single compact platform. Overall, temporal averaging substantially reduces random measurement noise while maintaining minute-scale temporal resolution for ambient observations.

https://doi.org/10.5194/egusphere-2026-5836
Preprint. Discussion started: 3 November 2026
© Author(s) 2026. CC BY 4.0 License.

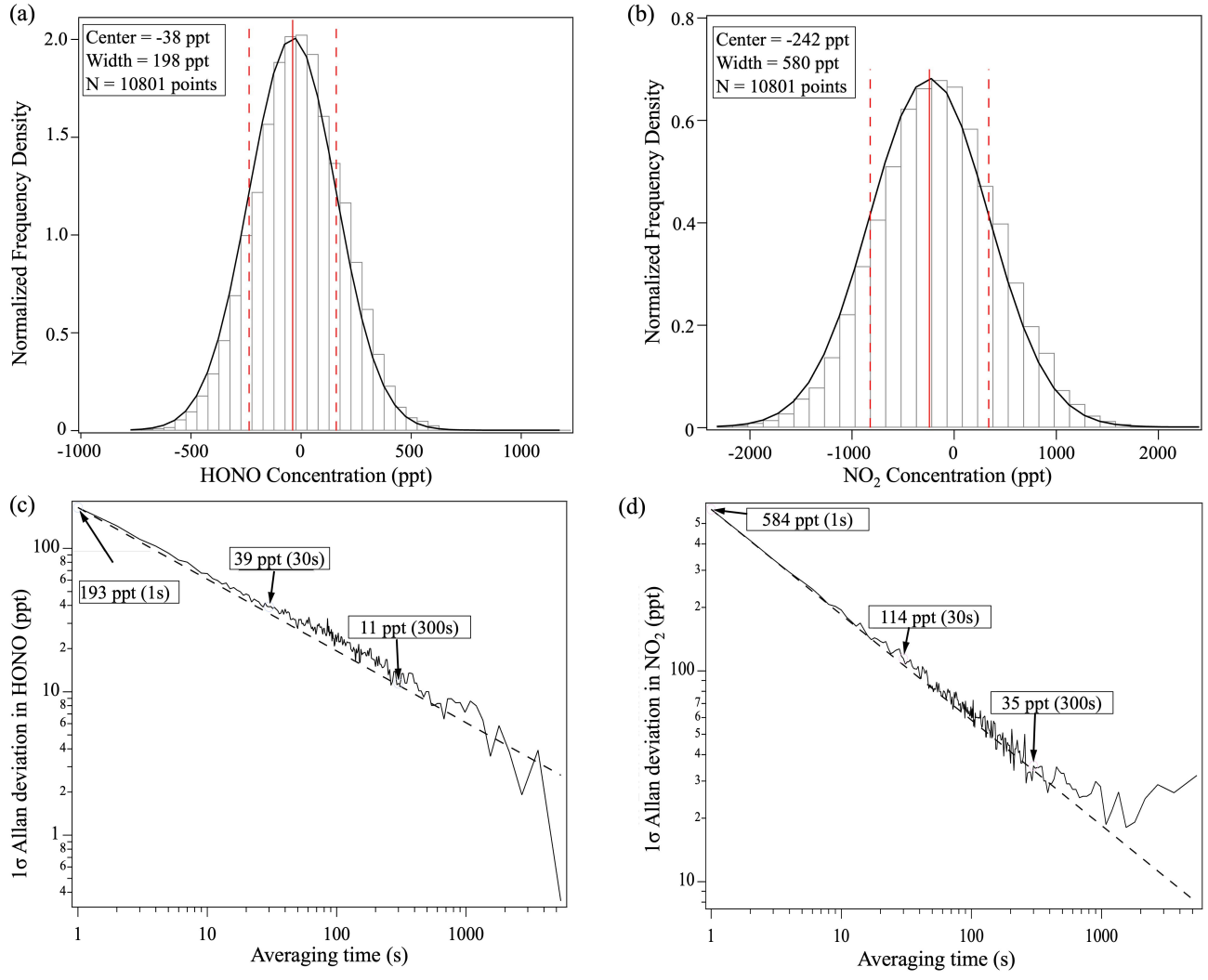


Figure 3: Precision and short-term stability of the BBCEAS measurements under zero-air conditions in the laboratory. (a, b) Normalized concentration distributions and Gaussian fits for HONO and NO_2, respectively. The solid red lines indicate the fitted mean concentrations, and the dashed red lines indicate ±1σ. (c, d) Allan deviations of HONO and NO_2 as a function of averaging time. The dashed lines represent the $\tau^{-1/2}$ dependence expected for white noise.

Table 1. Comparison of representative BBCEAS instruments for HONO and NO_2 measurements

Study	Species	Weight	Time Resolution	Precision
This work	HONO, NO_2	9 kg (19 lb)	60 s	60 ppt HONO, 152 ppt NO_2 (2σ)
This work	HONO, NO_2	9 kg (19 lb)	1 s	193 ppt HONO, 584 ppt NO_2 (1σ)
Duan *et al.*, 2018	HONO, NO_2	Not reported	30 s	180 ppt HONO, 340 ppt NO_2 (2σ)
Tang *et al.*, 2020	HONO, NO_2	Not reported	60 s	80 ppt HONO, 140 ppt NO_2 (2σ)
Womack *et al.*, 2022	Only NO_2	3.05 kg (6.7 lb)	1 s	43 ppt NO_2 (1σ)

https://doi.org/10.5194/egusphere-2026-5836
Preprint. Discussion started: 3 November 2026
© Author(s) 2026. CC BY 4.0 License.

4.2 Intercomparison of measurements

We evaluated BBCEAS performance by comparing its measurements with independent reference methods for HONO and NO_2 over atmospherically relevant concentration ranges.

For HONO, gaseous HONO was generated using the laboratory source described in Sect. 2.6. Measurements were made simultaneously with the BBCEAS and a Thermo Scientific Model 42i chemiluminescence NO_x analyzer. The Model 42i measures NO by ozone chemiluminescence and determines NO_x using a heated molybdenum converter. Following Chai et al. (2019), the increase in NO_x concentration relative to the zero-air baseline was used as the reference HONO concentration.

As shown in Fig. 4a, the BBCEAS measurements agreed closely with the reference values over the range of 0-65000 ppt. Linear regression gave a slope of 1.0093, an intercept of -6.145 ppt, and $R^2 = 0.9994$. The slope close to unity and the near-zero intercept indicate good agreement in both concentration response and baseline between the two methods. The linear response over the full concentration range also indicates that the BBCEAS retrieval remained linear under these experimental conditions.

The NO_2 response was evaluated separately using a certified 20 ppm NO_2 standard (Airgas, USA), which was dynamically diluted with zero air using an automated gas dilution system (Ecotech GasCal 1100, Australia). The diluted NO_2 was measured simultaneously with the BBCEAS and an Ecotech Serinus 60 NO_2 analyzer. The Serinus 60 uses cavity attenuated phase shift (CAPS) spectroscopy to determine NO_2 concentrations from the optical extinction associated with NO_2 absorption in a high-reflectivity cavity (Kebabian et al., 2005; Kebabian et al., 2008). The two instruments showed a strong linear relationship over the investigated NO_2 concentration range (Fig. 4b). Linear regression yielded a slope of 0.9662, an intercept of -287.42 ppt, and $R^2 = 0.9971$. The slope close to unity indicates consistent concentration responses between the BBCEAS and CAPS measurements. The negative intercept represents a concentration-independent offset between the two measurements, which is more apparent at the lower end of the concentration range.

Overall, the intercomparison results show that the BBCEAS provides a linear response and good agreement with the reference methods for both HONO and NO_2 over the concentration ranges investigated.

https://doi.org/10.5194/egusphere-2026-5836
Preprint. Discussion started: 3 November 2026
© Author(s) 2026. CC BY 4.0 License.

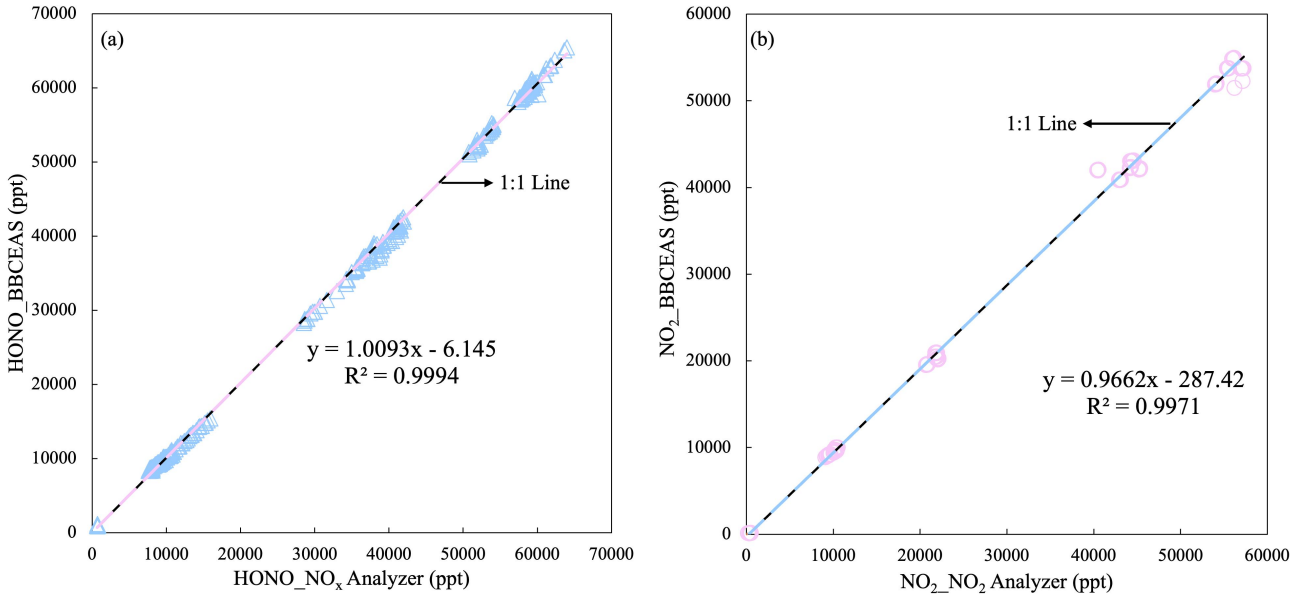


Figure 4: Intercomparison of BBCEAS-derived HONO and NO_2 concentrations with reference analyzers. (a) Comparison of HONO concentrations measured by BBCEAS and a NO_x analyzer. (b) Comparison of NO_2 concentrations measured by BBCEAS and a NO_2 analyzer.

4.3 Influence of Water Vapor on HONO and NO_2 Measurements

Water vapor is an important variable in atmospheric environments and can influence both optical measurements and heterogeneous processes involving HONO and NO_2 (Finlayson-Pitts et al., 2003; Spataro and Ianniello, 2014). In cavity-enhanced absorption measurements, changes in water-vapor content may alter optical extinction and spectral baselines, while variations in humidity can also affect heterogeneous HONO-NO_2 conversion processes occurring on sampling surfaces (Ball and Jones, 2003; Min et al., 2016; Washenfelder et al., 2008). Therefore, the robustness of BBCEAS measurements under different water-vapor conditions was evaluated using controlled humidification experiments.

A humidity-conditioning unit was installed upstream of the BBCEAS inlet. The system consisted of parallel dry and humidified flow paths operated at a constant total flow rate. Four water-vapor conditions were generated by varying the dry fraction (0, 1/3, 2/3, and 1), where increasing dry fraction corresponds to decreasing water-vapor content. Measurements obtained at each condition were compared with those acquired under the fully humidified condition (dry fraction = 0). The relative bias was calculated as

$$\text{Relative Bias (\%)} = \frac{C_i - C_0}{C_0} \times 100\%, \quad (6)$$

where C_i is the concentration measured at a given dry fraction, and C_0 is the concentration measured at dry fraction = 0.

HONO measurements were conducted at two concentration levels (approximately 37000 and 700 pptv) using the HONO generation system described in Sect. 2.6. The relative biases remained within ±2 % for the high-concentration measurements and within ±4 % for the low-concentration measurements (Fig. 5a). No systematic dependence on dry fraction was observed

https://doi.org/10.5194/egusphere-2026-5836
Preprint. Discussion started: 3 November 2026
© Author(s) 2026. CC BY 4.0 License.

for either concentration level, indicating that variations in water-vapor content did not introduce a measurable bias into the HONO retrieval.

Simultaneously retrieved NO_2 concentrations during the HONO experiments remained close to zero under all dry-fraction conditions. Retrieved NO_2 concentrations ranged from approximately -426 to 373 pptv and showed no systematic dependence on dry fraction. These values are comparable to the baseline variability observed under zero-air conditions and provide no evidence for significant humidity-dependent NO_2 formation within the sampling system.

Influence of water vapor on NO_2 retrievals was evaluated independently using NO_2 concentrations of approximately 10000, 20000, 45000, and 55000 pptv. As shown in Fig. 5b, the relative biases generally remained within ±4 % of the reference condition. Although small fluctuations were observed at individual dry-fraction conditions, no systematic dependence on dry fraction was evident for any concentration level. The mean relative bias remained close to zero throughout the experiment, indicating that the effect of water-vapor variations on NO_2 retrievals was minor.

The mean HONO/NO_2 ratios were below 0.05 for all NO_2 concentrations and dry-fraction conditions during the NO_2 experiments (Fig. 5c), with no consistent trend as water-vapor content changed. The low and stable HONO levels indicate that measurable conversion of NO_2 to HONO did not occur within the sampling system. Because HONO formation from NO_2 is typically attributed to heterogeneous surface reactions that require finite reaction times (Finlayson-Pitts et al., 2003; Kleffmann, 2007), the short residence time of the sampling system (<2 s) likely limited any in situ HONO production to below measurable levels.

Overall, the biases observed for both HONO and NO_2 were small and showed no systematic dependence on dry fraction. In addition, neither experiment provided evidence for measurable humidity-driven conversion between HONO and NO_2. The results indicate that the influence of water vapor on HONO and NO_2 retrievals is minor under the conditions investigated, supporting the use of the BBCEAS instrument over a wide range of atmospheric humidity conditions.

https://doi.org/10.5194/egusphere-2026-5836
Preprint. Discussion started: 3 November 2026
© Author(s) 2026. CC BY 4.0 License.

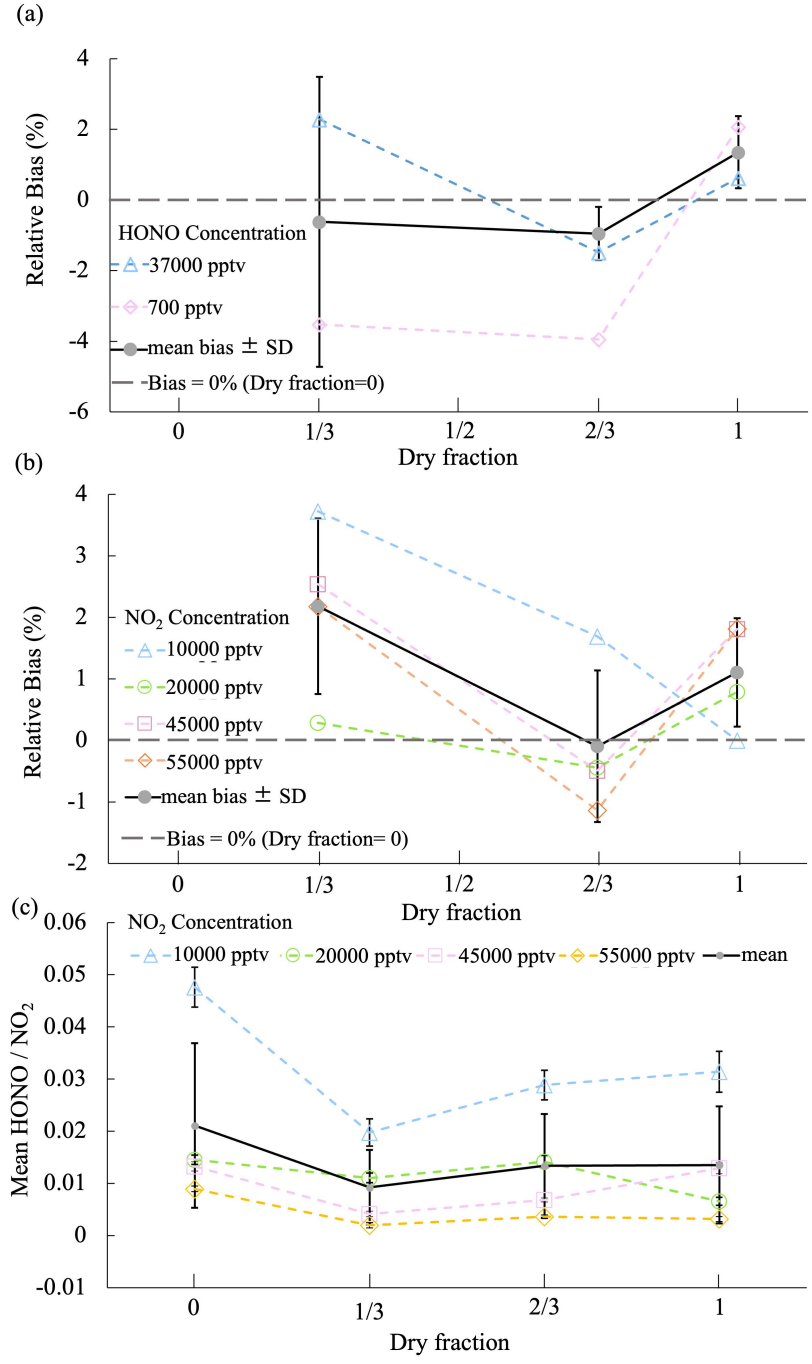


Figure 5: An example for accurate data representation & universal readability of figures.Influence of water-vapor conditions on BBCEAS HONO and NO_2 measurements. (a) Relative bias of HONO measurements at two concentration levels (~37000 and ~700 pptv). (b) Relative bias of NO_2 measurements at four concentration levels (10000, 20000, 45000, and 55000 pptv). Black symbols denote the mean relative bias, and error bars denote ±1 SD. (c) HONO/NO_2 ratios during the NO_2 experiments. Colored symbols represent individual NO_2 concentrations, and black symbols represent the mean HONO/NO_2 ratio (±1 SD). Relative biases in (a) and (b) are referenced to the measurements at dry fraction = 0.

https://doi.org/10.5194/egusphere-2026-5836
Preprint. Discussion started: 3 November 2026
© Author(s) 2026. CC BY 4.0 License.

4.4 Demonstration of ambient HONO and NO_2 measurements

We performed continuous measurements of HONO and NO_2 in Syracuse, New York, from 17:00 LT on 28 July to 17:00 LT on 29 July 2026. The following analysis is based on 60 s averaged data unless otherwise indicated.

The instrument operated continuously throughout the deployment without interruption. HONO concentrations ranged from approximately 15 to 520 pptv, while NO_2 concentrations ranged from approximately 430 to 6700 pptv. The measured concentration changes were substantially greater than the instrumental uncertainty determined in Sect. 4.1, demonstrating that the instrument was capable of resolving real atmospheric variability in both species.

As shown in Fig. 6, both HONO and NO_2 exhibited pronounced temporal variability over the course of the measurement period, while HONO/NO_2 ratios ranged from near zero to approximately 0.4. Periods of enhanced HONO were associated with elevated HONO/NO_2 ratios, indicating changes in the relative abundance of the two species rather than simple co-variability with NO_2. During the evening enhancement period (19:00–21:00 LT), mean HONO and NO_2 concentrations were 258 ± 67 pptv and 2551 ± 1097 pptv, respectively, corresponding to a mean HONO/NO_2 ratio of 0.12 ± 0.06. In contrast, the broader nighttime period (21:00–06:00 LT) was characterized by lower HONO concentrations (74 ± 7 pptv) and comparatively stable HONO/NO_2 ratios despite sustained NO_2 levels (2490 ± 799 pptv).

The most prominent feature of the record was a pre-sunrise HONO enhancement between approximately 05:00 and 06:00 LT, when HONO concentrations briefly exceeded 500 pptv and HONO/NO_2 ratios reached 0.3–0.4. Following sunrise, both HONO concentrations and HONO/NO_2 ratios decreased rapidly. Similar behavior has been reported in previous field studies and it can be generally attributed to nocturnal HONO accumulation followed by rapid photolytic loss after sunrise (Stutz et al., 2004; Wong et al., 2011).

The HONO/NO_2 ratio exhibited clear diurnal variability. Ratios were generally below 0.1 during most daytime periods but increased substantially during the evening accumulation event and the pre-sunrise enhancement. The observed HONO/NO_2 ratios typically ranged from 0.02 to 0.20, with short-lived peaks approaching 0.5. These values are comparable to those reported in urban and suburban boundary-layer environments (Stutz et al., 2004; Wang et al., 2025a; Wong et al., 2011), supporting the atmospheric plausibility of the retrieved HONO concentrations.

The observations captured characteristic temporal variability in ambient HONO and NO_2, including an evening HONO accumulation event, enhanced HONO/NO_2 ratios before sunrise, and lower daytime HONO abundances. No baseline drift, concentration discontinuities, or evidence of instrumental instability were observed throughout the measurement period. Combined with the laboratory characterization presented above, the field measurements demonstrate that the BBCEAS instrument is capable of reliable, continuous monitoring of atmospheric HONO and NO_2 under ambient conditions.

https://doi.org/10.5194/egusphere-2026-5836
Preprint. Discussion started: 3 November 2026
© Author(s) 2026. CC BY 4.0 License.

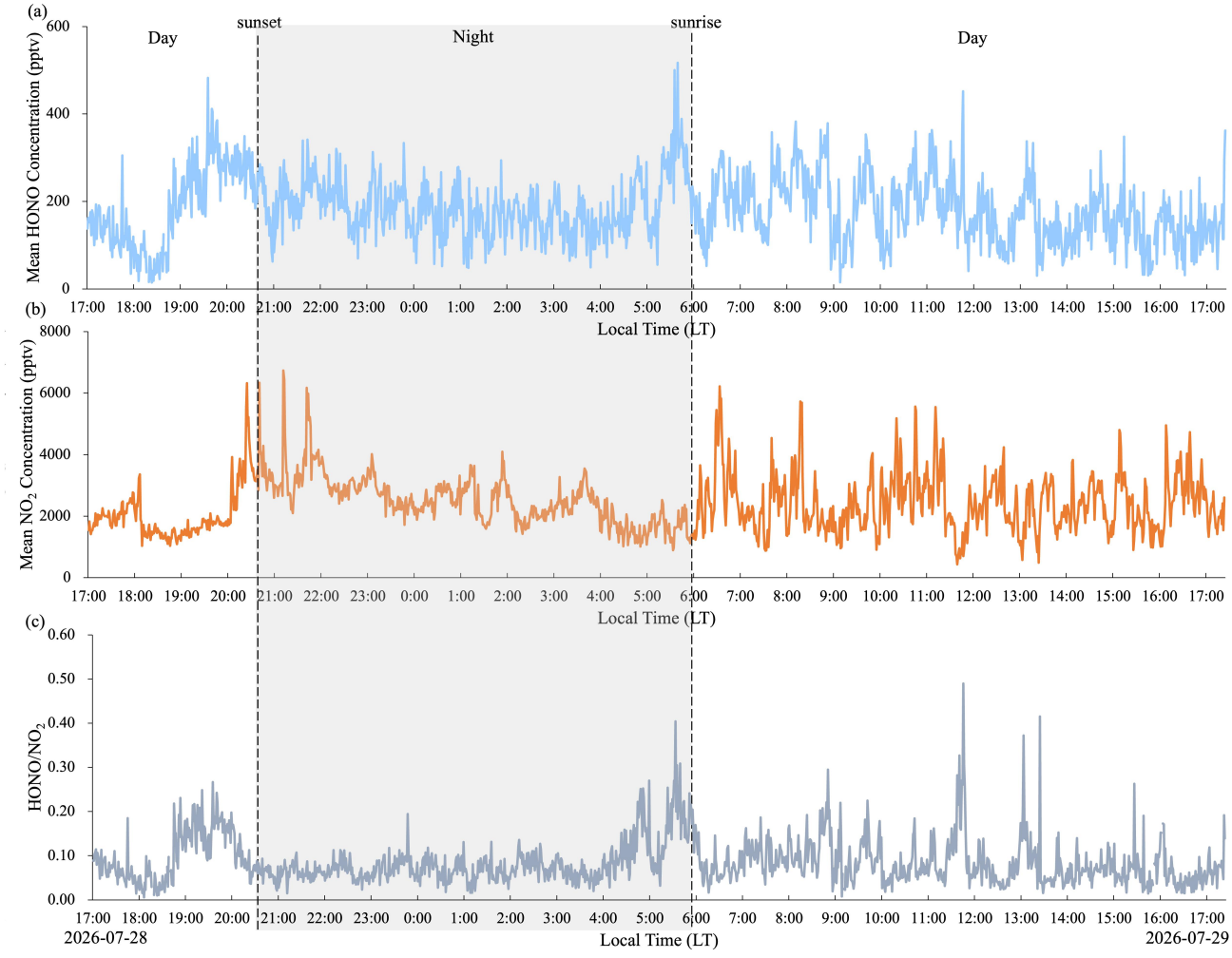


Figure 6: Time series of mean HONO concentration (a), mean NO_2 concentration (b), and the HONO/NO_2 ratio (c) measured by the BBCEAS system during a 24 h field deployment in Syracuse, New York, from 17:00 LT on 28 July to 17:00 LT on 29 July 2026. The shaded region denotes nighttime conditions between local sunset and sunrise. The 60 s instrument precisions determined from Allan deviation analysis were 30 ppt for HONO and 76 ppt for NO_2.

5 Conclusions and future work

A broadband cavity-enhanced absorption spectrometer (BBCEAS) was developed for simultaneous measurements of atmospheric HONO and NO_2 in the near-UV spectral region. The instrument employs cavity mirrors with a measured reflectivity of 0.99986 at 368 nm and a rapid spectral acquisition scheme with an integration time of 0.15 s. Zero-air measurements and Allan variance analysis demonstrated stable performance, with 1σ precisions of 193 pptv for HONO and 584 pptv for NO_2 at 1 s. With 60 s averaging, the corresponding precisions improved to approximately 30 and 76 pptv, respectively, yielding 2σ detection limits estimated from the measurement precision of approximately 60 and 152 pptv,

https://doi.org/10.5194/egusphere-2026-5836
Preprint. Discussion started: 3 November 2026
© Author(s) 2026. CC BY 4.0 License.

respectively. Intercomparison measurements showed excellent agreement with reference analyzers for both HONO and NO_2, with regression slopes of 1.0093 and 0.9662 and R^2 values of 0.9994 and 0.9971, respectively. Controlled humidity experiments showed no systematic dependence of the retrieved HONO and NO_2 concentrations on water vapour over the investigated range, indicating robust performance under the tested conditions. A 24 h ambient deployment in Syracuse, New York, further demonstrated the capability of the instrument to continuously measure HONO and NO_2 under field conditions. The instrument operated without interruption and resolved substantial temporal variability in both species, including pptv-level HONO concentrations. These observations confirmed that the measurement performance established under laboratory conditions was maintained during ambient operation.

The resulting instrument enables simultaneous HONO and NO_2 measurements on a compact platform suitable for stationary and mobile applications and provides a basis for extending reactive nitrogen measurements to environments where conventional instrumentation is difficult to deploy. Future applications of the BBCEAS instrument will focus on long-term observations in urban, suburban, rural, coastal, and forested environments to investigate the spatiotemporal variability of HONO and NO_2 under different atmospheric conditions. The instrument may also be deployed on mobile platforms to support regional mapping studies and satellite validation efforts. Such measurements will help improve understanding of HONO sources and sinks, HONO-NO_2 relationships, and the role of reactive nitrogen chemistry in atmospheric oxidation processes.

Code and data availability

Code and data used are available upon request (jichai@esf.edu).

Author contributions

Yilan, Caroline, and Jiajue designed and built the instrument. Yilan performed the measurements, analyzed the data, prepared the figures, and wrote the manuscript. Nell, Caroline, and Jiajue contributed to manuscript review and editing. Jiajue provided supervision and acquired funding for the project. All authors discussed the results and approved the final manuscript.

Competing interests

The authors declare that they have no competing interests.

https://doi.org/10.5194/egusphere-2026-5836
Preprint. Discussion started: 3 November 2026
© Author(s) 2026. CC BY 4.0 License.

Disclaimer

Copernicus Publications adds a standard disclaimer: "Copernicus Publications remains neutral with regard to jurisdictional claims made in the text, published maps, institutional affiliations, or any other geographical representation in this paper. While Copernicus Publications makes every effort to include appropriate place names, the final responsibility lies with the authors. Views expressed in the text are those of the authors and do not necessarily reflect the views of the publisher."

Acknowledgements

Besides the author's statement of gratitude to and recognition of the people and institutions that helped the author's research and writing, authors are also asked to include relevant research infrastructure they have benefitted from during their research, where research was conducted or data/resources were used. Examples are Field Stations and Marine Laboratories (FSMLs).We are grateful to Paul Theroux of RI-DEM/RI-DOH for access and support at the RI-DEM air-monitoring site and for providing data from these sites for our analyses. We thank Greyson Flynn and Lyn Lin for their assistance with field deployment and ambient measurements using the BBCEAS instrument. We thank the National Science Foundation for funding (award no. AGS 2331252 and AGS 2305090 to JC) and SUNY ESF for funding to JC.

Financial support

This research has been supported by the National Science Foundation AGS 2331252 and AGS 2305090.

References

Alicke, B., A. Geyer, A. Hofzumahaus, F. Holland, S. Konrad, H. Pätz, J. Schäfer, J. Stutz, A. Volz-Thomas & U. Platt (2003) OH formation by HONO photolysis during the BERLIOZ experiment. *Journal of Geophysical Research: Atmospheres,* 108**,** PHO 3–1–PHO 3–17.

Andersen, S. T., L. J. Carpenter, C. Reed, J. D. Lee, R. Chance, T. Sherwen, A. R. Vaughan, J. Stewart, P. M. Edwards & W. J. Bloss (2023) Extensive field evidence for the release of HONO from the photolysis of nitrate aerosols. *Science Advances,* 9**,** eadd6266.

Aubin, D. G. & J. P. Abbatt (2007) Interaction of NO_2 with hydrocarbon soot: Focus on HONO yield, surface modification, and mechanism. *The Journal of Physical Chemistry A,* 111**,** 6263–6273.

Ball, S. M. & R. L. Jones (2003) Broad-band cavity ring-down spectroscopy. *Chemical reviews,* 103**,** 5239–5262.

Bao, F., Y. Cheng, U. Kuhn, G. Li, W. Wang, A. M. Kratz, J. Weber, B. Weber, U. Po¨ schl & H. Su (2022) Key role of equilibrium HONO concentration over soil in quantifying soil–atmosphere HONO fluxes. *Environmental science & technology,* 56**,** 2204–2212.

https://doi.org/10.5194/egusphere-2026-5836
Preprint. Discussion started: 3 November 2026
© Author(s) 2026. CC BY 4.0 License.

Chai, J., D. J. Miller, E. Scheuer, J. Dibb, V. Selimovic, R. Yokelson, K. J. Zarzana, S. S. Brown, A. R. Koss, C. Warneke & M. Hastings (2019) Isotopic characterization of nitrogen oxides (NO_x), nitrous acid (HONO), and nitrate (pNO_3^-) from laboratory biomass burning during FIREX. *Atmospheric Measurement Techniques,* 12**,** 6303–6317.

Crilley, L. R., L. J. Kramer, B. Ouyang, J. Duan, W. Zhang, S. Tong, M. Ge, K. Tang, M. Qin, P. Xie, M. D. Shaw, A. C. Lewis, A. Mehra, T. J. Bannan, S. D. Worrall, M. Priestley, A. Bacak, H. Coe, J. Allan, C. J. Percival, O. A. M. Popoola, R. L. Jones & W. J. Bloss (2019) Intercomparison of nitrous acid (HONO) measurement techniques in a megacity (Beijing). *Atmos. Meas. Tech.,* 12**,** 6449–6463.

Duan, J., M. Qin, B. Ouyang, W. Fang, X. Li, K. Lu, K. Tang, S. Liang, F. Meng, Z. Hu, P. Xie, W. Liu & R. Häsler (2018) Development of an incoherent broadband cavity-enhanced absorption spectrometer for in situ measurements of HONO and NO_2. *Atmos. Meas. Tech.,* 11**,** 4531–4543.

Fiedler, S. E., A. Hese & A. A. Ruth (2003) Incoherent broad-band cavity-enhanced absorption spectroscopy. *Chemical Physics Letters,* 371**,** 284–294.

Finlayson-Pitts, B., L. Wingen, A. Sumner, D. Syomin & K. Ramazan (2003) The heterogeneous hydrolysis of NO_2 in laboratory systems and in outdoor and indoor atmospheres: An integrated mechanism. *Physical Chemistry Chemical Physics,* 5**,** 223–242.

Gherman, T., D. S. Venables, S. Vaughan, J. Orphal & A. A. Ruth (2008) Incoherent Broadband Cavity-Enhanced Absorption Spectroscopy in the near-Ultraviolet:
Application to HONO and NO_2. *Environmental science & technology,* 42**,** 890–895.

Gingerysty, N. J. & H. D. Osthoff (2020) A compact, high-purity source of HONO validated by Fourier transform infrared and thermal-dissociation cavity ring-down spectroscopy. *Atmospheric Measurement Techniques,* 13**,** 4159–4167.

Harper, A. P., C. E. Flowerday, Z. Giauque, K. Brewster, R. Thalman & J. C. Hansen (2025) High-purity nitrous acid (HONO) generation and quantification using broadband cavity-enhanced absorption spectroscopy (BBCEAS). *Atmospheric Measurement Techniques,* 18**,** 7221–7230.

Heland, J., J. Kleffmann, R. Kurtenbach & P. Wiesen (2001) A new instrument to measure gaseous nitrous acid (HONO) in the atmosphere. *Environmental Science & Technology,* 35**,** 3207–3212.

Kebabian, P. L., S. C. Herndon & A. Freedman (2005) Detection of nitrogen dioxide by cavity attenuated phase shift spectroscopy. *Analytical chemistry,* 77**,** 724–728.

Kebabian, P. L., E. C. Wood, S. C. Herndon & A. Freedman (2008) A practical alternative to chemiluminescence-based detection of nitrogen dioxide: Cavity attenuated phase shift spectroscopy. *Environmental science & technology,* 42**,** 6040–6045.

Kennedy, O. J., B. Ouyang, J. M. Langridge, M. J. S. Daniels, S. Bauguitte, R. Freshwater, M. W. McLeod, C. Ironmonger, J. Sendall, O. Norris, R. Nightingale, S. M. Ball & R. L. Jones (2011) An aircraft based three channel broadband cavity enhanced absorption spectrometer for simultaneous measurements of NO_3, N_2O_5 and NO_2. *Atmos. Meas. Tech.,* 4**,** 1759–1776.

https://doi.org/10.5194/egusphere-2026-5836
Preprint. Discussion started: 3 November 2026
© Author(s) 2026. CC BY 4.0 License.

Kim, K., K. M. Han, C. H. Song, H. Lee, R. Beardsley, J. Yu, G. Yarwood, B. Koo, J. Madalipay & J.-H. Woo (2024) An investigation into atmospheric nitrous acid (HONO) processes in South Korea. *Atmospheric Chemistry and Physics,* 24**,** 12575–12593.

Kleffmann, J. (2007) Daytime sources of nitrous acid (HONO) in the atmospheric boundary layer. *ChemPhysChem,* 8**,** 1137–1144.

Kleffmann, J., T. Gavriloaiei, A. Hofzumahaus, F. Holland, R. Koppmann, L. Rupp, E. Schlosser, M. Siese & A. Wahner (2005) Daytime formation of nitrous acid: A major source of OH radicals in a forest. *Geophysical Research Letters,* 32.

Kleffmann, J. & P. Wiesen (2008) Technical Note: Quantification of interferences of wet chemical HONO LOPAP measurements under simulated polar conditions. *Atmos. Chem. Phys.,* 8**,** 6813–6822.

Langridge, J. M., S. M. Ball, A. J. Shillings & R. L. Jones (2008) A broadband absorption spectrometer using light emitting diodes for ultrasensitive, in situ trace gas detection. *Review of scientific instruments,* 79.

Langridge, J. M., Laurila, T., Watt, R. S., Jones, R. L., Kaminski, C. F., Hult, J. (2008) Cavity enhanced absorption spectroscopy of multiple trace gas species using a supercontinuum radiation source. *Optics Express* 16**,** 10178–10188.

Lao, M., L. R. Crilley, L. Salehpoor, T. C. Furlani, I. Bourgeois, J. A. Neuman, A. W. Rollins, P. R. Veres, R. A. Washenfelder & C. C. Womack (2020) A portable, robust, stable, and tunable calibration source for gas-phase nitrous acid (HONO). *Atmospheric Measurement Techniques,* 13**,** 5873–5890.

Levenberg, K. (1944) A method for the solution of certain non-linear problems in least squares. *Quarterly of applied mathematics,* 2**,** 164–168.

Marquardt, D. W. (1963) An algorithm for least-squares estimation of nonlinear parameters. *Journal of the society for Industrial and Applied Mathematics,* 11**,** 431–441.

Min, K. E., R. A. Washenfelder, W. P. Dubé, A. O. Langford, P. M. Edwards, K. J. Zarzana, J. Stutz, K. Lu, F. Rohrer, Y. Zhang & S. S. Brown (2016) A broadband cavity enhanced absorption spectrometer for aircraft measurements of glyoxal, methylglyoxal, nitrous acid, nitrogen dioxide, and water vapor. *Atmospheric Measurement Techniques,* 9**,** 423–440.

Pinto, J., J. Dibb, B. Lee, B. Rappenglück, E. Wood, M. Levy, R. Y. Zhang, B. Lefer, X. R. Ren & J. Stutz (2014) Intercomparison of field measurements of nitrous acid (HONO) during the SHARP campaign. *Journal of Geophysical Research: Atmospheres,* 119**,** 5583–5601.

Roberts, J. M., P. Veres, C. Warneke, J. A. Neuman, R. A. Washenfelder, S. S. Brown, M. Baasandorj, J. B. Burkholder, I. R. Burling, T. J. Johnson, R. J. Yokelson & J. de Gouw (2010) Measurement of HONO, HNCO, and other inorganic acids by negative-ion proton-transfer chemical-ionization mass spectrometry (NI-PT-CIMS): application to biomass burning emissions. *Atmos. Meas. Tech.,* 3**,** 981–990.

Spataro, F. & A. Ianniello (2014) Sources of atmospheric nitrous acid: State of the science, current research needs, and future prospects. *Journal of the Air & Waste Management Association,* 64**,** 1232–1250.

Stemmler, K., M. Ammann, C. Donders, J. Kleffmann & C. George (2006) Photosensitized reduction of nitrogen dioxide on humic acid as a source of nitrous acid. *Nature,* 440**,** 195–198.

https://doi.org/10.5194/egusphere-2026-5836
Preprint. Discussion started: 3 November 2026
© Author(s) 2026. CC BY 4.0 License.

Stutz, J., B. Alicke, R. Ackermann, A. Geyer, S. Wang, A. B. White, E. J. Williams, C. W. Spicer & J. D. Fast (2004) Relative humidity dependence of HONO chemistry in urban areas. *Journal of Geophysical Research: Atmospheres,* 109.

Stutz, J., E. Kim, U. Platt, P. Bruno, C. Perrino & A. Febo (2000) UV-visible absorption cross sections of nitrous acid. *Journal of Geophysical Research: Atmospheres,* 105**,** 14585–14592.

Tang, K., M. Qin, W. Fang, J. Duan, F. Meng, K. Ye, H. Zhang, P. Xie, Y. He, W. Xu, J. Liu & W. Liu (2020) Simultaneous detection of atmospheric HONO and NO_2 utilising an IBBCEAS system based on an iterative algorithm. *Atmos. Meas. Tech.,* 13**,** 6487–6499.

Thalman, R., K. J. Zarzana, M. A. Tolbert & R. Volkamer (2014) Rayleigh scattering cross-section measurements of nitrogen, argon, oxygen and air. *Journal of Quantitative Spectroscopy and Radiative Transfer,* 147**,** 171–177.

Vandaele, A. C., C. Hermans, P. C. Simon, M. Carleer, R. Colin, S. Fally, M.-F. Merienne, A. Jenouvrier & B. Coquart (1998) Measurements of the NO_2 absorption cross-section from 42 000 cm^{-1} to 10 000 cm^{-1} (238–1000 nm) at 220 K and 294 K. *Journal of Quantitative Spectroscopy and Radiative Transfer,* 59**,** 171–184.

Veres, P., J. M. Roberts, C. Warneke, D. Welsh-Bon, M. Zahniser, S. Herndon, R. Fall & J. de Gouw (2008) Development of negative-ion proton-transfer chemical-ionization mass spectrometry (NI-PT-CIMS) for the measurement of gas-phase organic acids in the atmosphere. *International Journal of Mass Spectrometry,* 274**,** 48–55.

Wang, L., J. Chai, B. Gaubert & Y. Huang (2025a) A review of measurements and model simulations of atmospheric nitrous acid. *Atmospheric Environment,* 347**,** 121094.

Wang, M., W. Liu, X. Ding, T. Liu, W. Zhou, S. Lou, D. S. Venables, R. Varma, C. Huang & J. Chen (2025b) Rapid and high-precision cavity-enhanced spectroscopic measurement of HONO and NO_2: Application to emissions from heavy-duty diesel vehicles in chassis dynamometer tests and in mobile monitoring. *Talanta,* 285**,** 127386.

Washenfelder, R. A., A. O. Langford, H. Fuchs & S. S. Brown (2008) Measurement of glyoxal using an incoherent broadband cavity enhanced absorption spectrometer. *Atmos. Chem. Phys.,* 8**,** 7779–7793.

Werle, P. (2011) Accuracy and precision of laser spectrometers for trace gas sensing in the presence of optical fringes and atmospheric turbulence. *Applied Physics B,* 102**,** 313–329.

Werle, P. O., R. Mücke & F. Slemr (1993) The limits of signal averaging in atmospheric trace-gas monitoring by tunable diode-laser absorption spectroscopy (TDLAS). *Applied Physics B,* 57**,** 131–139.

Womack, C. C., S. S. Brown, S. J. Ciciora, R.-S. Gao, R. J. McLaughlin, M. A. Robinson, Y. Rudich & R. A. Washenfelder (2022) A lightweight broadband cavity-enhanced spectrometer for NO_2 measurement on uncrewed aerial vehicles. *Atmospheric Measurement Techniques,* 15**,** 6643–6652.

Wong, K. W., H. J. Oh, B. L. Lefer, B. Rappenglück & J. Stutz (2011) Vertical profiles of nitrous acid in the nocturnal urban atmosphere of Houston, TX. *Atmos. Chem. Phys.,* 11**,** 3595–3609.

Wu, T., W. Chen, E. Fertein, F. Cazier, D. Dewaele & X. Gao (2012) Development of an open-path incoherent broadband cavity-enhanced spectroscopy based instrument for simultaneous measurement of HONO and NO_2 in ambient air. *Applied Physics B,* 106**,** 501–509.

https://doi.org/10.5194/egusphere-2026-5836
Preprint. Discussion started: 3 November 2026
© Author(s) 2026. CC BY 4.0 License.



605 Zhang, Q., P. Liu, Y. Wang, C. George, T. Chen, S. Ma, Y. Ren, Y. Mu, M. Song & H. Herrmann (2023) Unveiling the underestimated direct emissions of nitrous acid (HONO). *Proceedings of the National Academy of Sciences,* 120**,** e2302048120.